ACS Macro Letters

Letter

pubs.acs.org/macroletters

Band Gap Opening in the Cycloaddition Functionalization of Carbon Nanotubes

Olayinka O. Ogunro,[†] Chantel I. Nicolas,[†] Eric A. Mintz,[†] and Xiao-Qian Wang*[,‡]

Departments of [†]Chemistry and [‡]Physics, Clark Atlanta University, Atlanta, Georgia 30314, United States

ABSTRACT: Covalent functionalization represents a promising avenue to tailor the electronic properties of carbon nanotubes. Recent experimental work has shown that cycloaddition of fluorinated olefins represents an effective approach to reduce the off-currents of mixed nanotube mats for transistor applications. We have studied the electronic structure characteristics of the corresponding [2 + 2] cycloaddition using dispersion-corrected density functional calculations. The band gap opening in chemically functionalized tubes is associated with the sp^2 to sp^3 rehybridization. Our calculation reveals that the experimentally observed suppression of metallic conductivity can be attributed to a symmetry aligned cycloaddition scheme that effectively transforms metallic tubes to semiconducting ones.

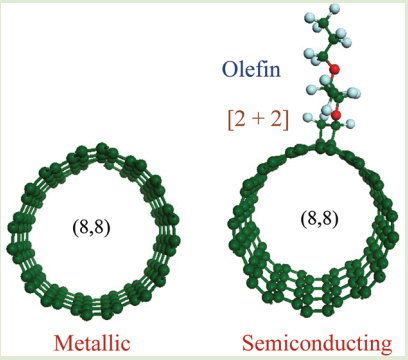

Single-walled carbon nanotubes (SWNTs) can be considered as graphene sheets rolled into a cylinder with unique electronic properties determined by their chiralities.[1,2] Both metallic and semiconducting SWNTs have widespread applications in nanoelectronics, molecular electronics, optoelectronics, drug delivery, and biochemical sensors.[3] Their applications are hampered by the fact that current synthetic methods produce bundles of nanotubes that are approximately one-third metallic and two-thirds semiconducting, and are extremely difficult to separate.[4] The presence of the metallic SWNTs results in undesirable high off-currents in transistor applications, while semiconducting nanotubes exhibit a substantial electrical response to the electrostatic and chemical gating effects that are desired for the function of chemical sensors and field effect transistors (FETs).[5]

Selective chemical conversion of metallic SWNTs to semiconducting ones would serve as a scalable alternative to separating SWNTs for transistor applications. To date, noncovalent functionalization of SWNTs has not been demonstrated to meet this need.[6−11] Covalent functionalization of SWNTs has been achieved via monovalent and divalent radical additions to the side walls of tubes.[12] Either addition causes a sp^2 to sp^3 rehybridization of the carbon atoms involved.[13−16] Monovalent functionalization via fluorination leads to highly reactive tubes with induced strains and fractures.[7] Recent experimental work by Kanungo and co-workers demonstrated that fluorinated olefins, perfluoro-(5-methyl-3,6-dioxanon-1-ene) (PMDE) and perfluoro-2(2-fluorosulfonylethoxy) propyl vinyl ether (PSEPVE), react with nanotube bundles via a [2 + 2] cycloaddition to yield an assemblage of tubes, which exhibits high-mobility semiconducting behavior free from metallic interference without the need of a separation step.[17] Although the side chains of the two olefins differ merely at the terminal group, the ionic mobility of PMDE-SWNT is ∼10 times higher than that of PSEPVE-SWNT. Kanungo and co-workers suggest that the SO_2F group leads to acid formation and doping.[17]

Despite the intriguing experimental findings, the mechanism of the exclusive conversion remains unclear. Specifically, it was suggested that the change from metallic to semiconducting behavior can be induced either through scattering centers associated with the covalent functionalization or through band structure modifications.[17] To facilitate an in-depth understanding of this mechanism, we have performed calculations based on density functional theory (DFT). Our results demonstrate that the cycloaddition functionalization leads to exclusive conversion from metallic tubes to semiconducting ones. In contrast, semiconducting nanotube features remain intact after functionalization. The cycloaddition of olefins involves an unusual thermally allowed [2 + 2] cycloaddition. Specifically, the highest occupied molecular orbital (HOMO) of the olefin, π, can interact with the conduction band of the nanotube, while the lowest unoccupied molecular level (LUMO) of the olefin, π^*, can interact with the valence band of the nanotube. Our results shed considerable light on the nature of the [2 + 2] cycloaddition with SWNTs.

We chose three prototypical tubes based on their high symmetry: (8,8), (14,0), and (15,0), which are metallic, semiconducting, and semimetallic, with diameters of 10.85, 10.96, and 11.17 Å, respectively. The structural and electronic properties were investigated using first-principles DFT. For the exchange-correlation the local Vosko−Wilk−Nusair (VWN)[18] functional and dispersion- and gradient-corrected (GGA) Perdew−Burke−Ernzerhof (PBE)[19] were used. The LDA-DFT approach is suitable for weakly interacting π systems while dispersion-corrected GGA provides a more accurate descrip-

Received: February 25, 2012
Accepted: April 2, 2012
Published: April 5, 2012

   dx.doi.org/10.1021/mz300091v | *ACS Macro Lett.* 2012, 1, 524−528

tion. Periodic-boundary conditions were employed with a supercell in the *xy* plane large enough to eliminate the interaction between neighboring replicas. A double numerical basis was sufficient for the grid integration of the charge density to converge. All structures were relaxed with forces less than 0.01 eV/Å.

Carbon atoms in graphene are sp^2-hybridized, with an extended conjugation forming a planar network. When graphene is rolled up to form a nanotube, the sp^2 hybridized orbitals are deformed due to rehybridization. When rolled up into a nanotube, graphene's sp^2 hybridized orbitals become misaligned for adjacent carbon atoms since the π orbitals of the nanotube are perpendicular to the tube's surface. Analogous to torsion strain in aromatic organic molecules, π orbital misalignment is the predominant source of strain in SWNTs.[20,21] The finite curvature of SWNTs determines electronic behavior by the (n,m) chiral index.[22] For a given (n,m), if $n = m$, the nanotube is metallic; if $n - m$ is a multiple of 3, then the nanotube is semimetallic; otherwise the nanotube is a semiconductor. The armchair (8,8) and zigzag tubes (14,0)/(15,0) were constructed with a unit cell of c = 9.84 and 12.78 Å, respectively.

We illustrate in Figure 1 the optimized structures of PMDE and PSEPVE functionalized armchair (8,8) tube formed by [2 + 2] cycloaddition. For (8,8), there are two distinctive adduct conformations, slanted or perpendicular to the tube axis. Similarly, (14,0) and (15,0) have two distinctive positions: parallel and slanted. As shown in Figure 1, adduct formation (yellow) distorts the tube surface by lifting the two carbon atoms attached to it. The bond length of each C−C bond within the four-membered ring is ∼1.54 Å, which is typical of sp^3 hybridized C−C bonds.[22−25] The four bonds connected to the adduct from the tube's surface are elongated to 1.49−1.50 Å. These results are summarized in Table 1.

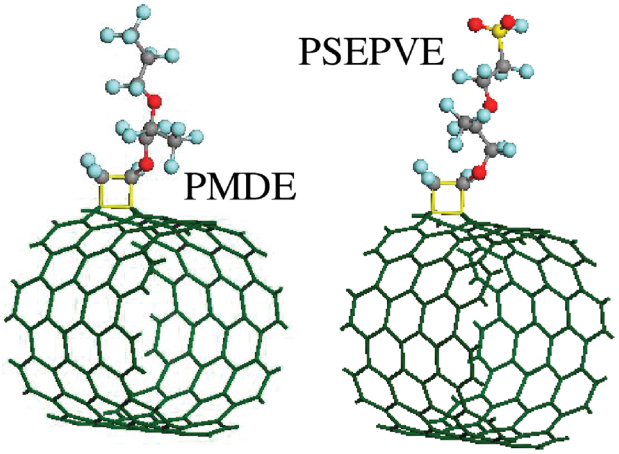

Figure 1. Perspective view of optimized structures of PMDE and PSEPVE functionalized armchair (8,8) tube, along with the adduct formed through [2 + 2] cycloaddition functionalization and the sp^3 rehybridized bonds on the tube. The red, light blue, gray, and yellow colored atoms represent oxygen, fluorine, carbon, and sulfur, respectively.

The calculated reaction path for [2 + 2] cycloaddition of PMDE-functionalized (8,8) tube is illustrated in Figure 2. The reactants are the olefin and the carbon nanotube. The product represents the formation of the adduct on the tube surface. The calculated transition barrier is ∼2.5 eV, slightly larger than calculated barrier for the addition of perfluorophenylazide to graphene (∼2 eV).[12] While the formation of the adduct weakly affects the transition barrier, it strongly impacts the energy of the product. Our calculation indicates that the formation of the cyclobutane adduct is endothermic as is expected. We have also calculated the transition barrier of a [4 + 2] cycloaddition, which is notably (∼2 eV) higher than that of the [2 + 2] cycloaddition. This supports the experimental assessment that the cycloaddition is of [2 + 2] type.

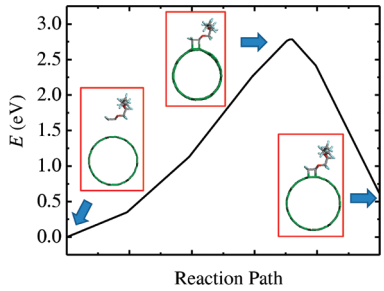

Figure 2. Calculated transition path for the [2 + 2] cycloaddition of PMDE-functionalized (8,8) tube.

For (8,8), the energy of slanted configuration is lower than perpendicular one by −0.6 eV (−1.1 eV) for LDA (dispersion-corrected PBE) calculations. Similarly, for (14,0) and (15,0), the LDA results indicate that parallel configuration is lower in energy than the slanted one by −0.1 and -0.3 eV, respectively. The corresponding energy differences for dispersion corrected PBE are −0.6 and −0.9 eV, respectively. The LDA and dispersion-corrected PBE approaches lead to the same energy trend. However, the dispersion-corrected PBE yields improved binding, which is attributed to the proper inclusion of long-range dispersion forces.

The local sp^3 rehybridization of the carbon atoms at the site of functionalization disrupts the π network. The functionalization site may act as a strong scattering center and a localized midgap state may emerge near the Fermi level. On the other hand, a strong hybridization among the molecular levels of the olefin and the bands of the SWNT may lead to intricate band alignments for the functionalized hybrid. Therefore, a detailed calculation of the band structure characteristics is useful to clarify the underlying mechanism.

To understand the site selectivity of the cylcoaddition reaction, we show in Figure 3 the calculated charge density of

Table 1. Calculated Electronic Properties of PMDE and PSEPVE Functionalized Nanotubes[a]

(n,m)	$E_g^{(0)}$ (eV)	$E_g^{(1)}$ (eV)	$E_g^{(2)}$ (eV)	d_1^{CC} (Å)	d_2^{CC} (Å)	d_1^{AD} (Å)	d_2^{AD} (Å)
(8,8)	0	0.2	0.21	1.49	1.50	1.55−1.62	1.54−1.59
(14,0)	0.65	0.41	0.23	1.49	1.49	1.55−1.62	1.55−1.62
(15,0)	0.02	0.15	0.10	1.49	1.50	1.55−1.57	1.55−1.57

[a]The labels (0), (1), and (2) refer to pristine, PMDE-, and PSEPVE-functionalized SWNTs, respectively.

dx.doi.org/10.1021/mz300091v | *ACS Macro Lett.* 2012, 1, 524−528

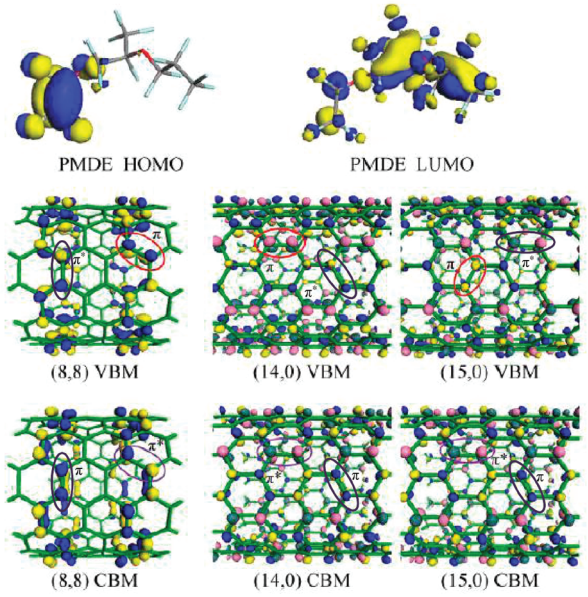

Figure 3. Isosurfaces of the wave functions of HOMO and LUMO for PMDE, along with those for VBM and CBM at the band center. The isovalue is 0.05 au.

near gap states of PMDE and (8,8), (14,0), and (15,0) SWNTs, respectively. The HOMO and LUMO of PMDE have π and π^* symmetry, respectively. For the (8,8) nanotube the valence band maximum (VBM) and conduction band minimum (CBM) exhibit adjacent p orbitals with both π and π^* symmetry. In the VBM adjacent perpendicular p orbitals exhibit π^* symmetry and adjacent slanted p orbitals exhibit π symmetry. This π and π^* symmetry is reversed for the CBM. Thus, symmetry allowed simultaneous $\pi-\pi^*$ interactions between the olefin and the nanotube yield a symmetry-allowed path. Similarly, for (14,0) and (15,0) VBM and CBM there are parallel and slanted π and π^* adjacent orbitals; however, the VBM and CBM are separated by an energy gap. Thus, the valence band and conduction band are both comprised of a sea of slightly misaligned p-orbitals. Both π and π^* local symmetries (circled) exist for each SWNT, whereby the VBM (occupied) and CBM (unoccupied) is allowed to interact with the PMDE HOMO and LUMO, respectively. In the valence band of the (8,8) tube, π symmetry is slanted relative to the axis, while π^* is perpendicular to the tube axis. For the conduction band, however, the π and π^* symmetries are perpendicular and slanted, respectively. For the valence band of the (14,0) tube, π symmetry is parallel with respect to the tube axis, while π^* is slanted. For the conduction band, however, the π and π^* symmetries are switched. For the (15,0) SWNT, the opposite is observed, whereby its valence band's π symmetry is slanted with respect to the tube axis, while π^* is parallel. Likewise, for the conduction band of (15,0), the positions of π and π^* symmetries are exchanged.

It is worth pointing out the distinctive charge distributions for PMDE and PSEPVE. Charge density confined to the chain end of PSEPVE creates a "tail" state, which is the lowest unoccupied state for PSEPVE (not shown). This flat state accounts for a crucial difference in electronic structure characteristics. The reactivity of the PSEPVE olefin is different from that of the PMDE olefin in that the LUMO of PSEPVE is confined to the fluorinated chain. Instead, the LUMO+1 state of PSEPVE has the proper π^* symmetry that can interact effectively with the VBM on the SWNTs.

Table 1 summarizes the structural and electronic features of functionalized tubes. The calculated band gaps (E_g) along with the corresponding bond lengths for the nearest neighbor C−C bonds (d^{CC}) and for the cycloaddition adduct (d^{AD}) for pristine and functionalized SWNTs. The armchair (8,8) was constructed with a unit cell of c = 9.84 Å, and the zigzag tubes (14,0) and (15,0) were constructed with unit cells of c = 12.78 Å. Upon functionalization of the armchair (8,8) tube the mirror symmetry is broken, causing the disruption of the π network. In the case of other functionalized tubes, despite differences in the side chain the atomic type and degree of symmetry breaking at the segment, the atoms in the side chain do not have a great influence on the band structures close to the Fermi level.[20] Furthermore, the PSEPVE functionalized tubes have smaller band gaps than PMDE functionalized counterparts. This feature is attributed to the emergence of a flat band, with charges predominantly confined at the tail of PSEPVE.

Cycloaddition on the nanotube surface leads to the disruption of π character. The resulting adduct opens up a band gap for metallic tubes. Summarized in Table 1 are the gaps extracted from band structure calculations. For (8,8), a gap of ∼0.2 eV emerges at the charge neutrality point (Fermi level). For (14,0) and (15,0) the gap decreases and increases, respectively. This is in conformity with the experimental results in that there is a preferred modification of electronic density-of-states for metallic tubes near the Fermi level.[17] The energy difference between the two distinct conformations is quantum in nature, as it is correlated to the degree of changes of the π network. For (8,8), the slanted conformation is lower in energy than the perpendicular one. This discrepancy in energy raises questions regarding the symmetry-allowed [2 + 2] cycloaddition. To illustrate this point, we show in Figure 3 the extracted isosurfaces of the PMDE olefin. It is known, at least for metallic SWNTs, that the VBM and CBM can be characterized as π and π^* bands, respectively. As seen in Figure 3, the local symmetry of the $p-p$ bond (circled) extracted at the band center (Γ point) for all three SWNTs. For (8,8) the π and π^* bands are singly degenerate. It is worth noting that the energetically preferred slanted conformation appears not to be symmetry allowed for [2 + 2] cylcoaddition since the allowed transition requires π interacting with π^*. Closer scrutiny of the charge density distributions at different k-points reveals that the local symmetry features change with respect to the k-point of the system. It is thus essential to study [2 + 2] addition via electronic structure characteristics based on periodic systems. As a result of the band structure, the symmetry allowed [2 + 2] always exists, albeit not necessarily at the band center. This is true for (8,8) and (15,0) as well. As such, there exists a crucial difference between conventional concerted [2 + 2] cycloaddion in molecular systems in view of the peculiar band feature.

The calculated band structures for each pristine nanotube and functionalized tube are displayed in Figure 4. For tube (8,8), a gap opens near the Fermi level. Careful examination of the band structures for pristine and functionalized nanotubes indicates that there are two dispersed bands involved near the Fermi level for PMDE, while there are three involved for PSEPVE. The band alignment between the pristine tube and the functionalized tube shows that HOMO and LUMO of the PMDE strongly hybridize into the valence band maximum (VBM) and conduction band minimum (CBM) states of the

dx.doi.org/10.1021/mz300091v | ACS Macro Lett. 2012, 1, 524−528

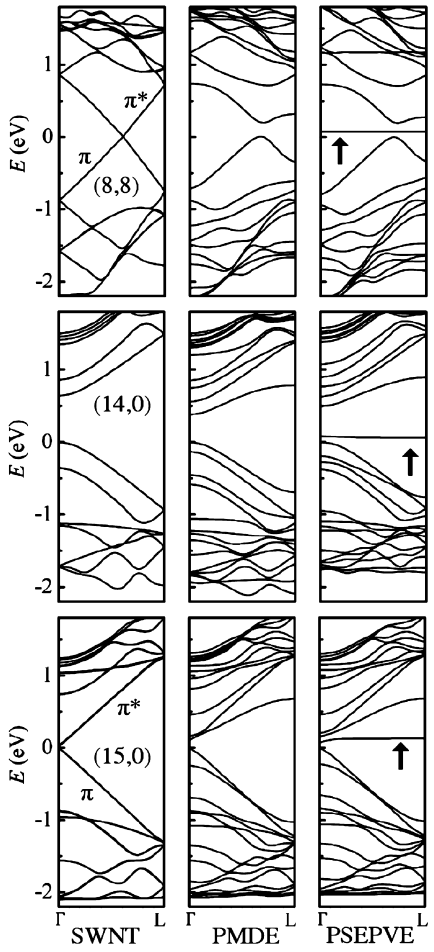

Figure 4. Calculated band structures for pristine (left column), PMDE functionalized (middle column), and PSEPVE functionalized (right column) armchair (8,8; top panel), zigzag (14,0; middle panel), and (15,0; bottom panel), respectively. The dashed line stands for the halfway between the valence band maximum (VBM) and conduction band minimum (CBM) of the pristine tubes that is set to zero for all cases.

pristine SWNTs. Conversely, PSEPVE has three levels involved.

For comparison, the band structure of each pristine tube, (8,8), (14,0), and (15,0), is displayed to the left of its corresponding PMDE and PSEPVE functionalized nanotubes. When PMDE is used to functionalize the semiconducting tube (14,0), attachment of the olefin to a C−C bond parallel to the tube axis results in a slightly larger band gap than when attached to a C−C bond slanted to the tube axis. For tube (15,0), functionalization parallel to the tube axis results in a small band gap at the band center, while functionalization in a position slanted to the tube axis leads to a small, nonzero band gap. The functionalization with PSEPVE yields a localized flat band near the Fermi level, which can be attributed to the sulfonyl side chain on the olefin. PSEPVE chemically functionalized nanotubes have an unoccupied level in the gap region; otherwise the band structure characteristics of PME- and PSEPVE-functionalzed tubes are nearly identical. The flat bands associated with this group are indicated by the arrows. It is important to note that for the metallic nanotube, there exists a symmetry allowed path that is not found at the Γ point, which is due to band structure continuity. However, for the semiconducting nanotube, neither change in symmetry nor band continuity exists. This is a key difference between metallic and semiconducting nanotubes. Our results are thus consistent with experimental findings concerning the reaction's preference to the (8,8) SWNTs.[17]

The formation of the cyclobutyl group onto the sidewall of the nanotube, results in different molecular symmetries at the site of bond formation. The charge density for the cyclobutyl group attached nanotube (15,0) is displayed in Figure 5. The nanotube bands affected by the olefin addition reaction are not close to the Fermi level. The HOMO-2 level was antisymmetric at the adduct as indicated by the blue and yellow wave functions. However, for HOMO-1, LUMO+2 and LUMO+4, each adduct is symmetric after the addition of the olefin. Despite the differences in symmetry, each HOMO and LUMO level leads to strong covalent bond formation between the nanotube and the fluorinated olefin. Similar results were reported by Cho and co-workers for carbon nanotubes functionalized with 1,3 dipoles via 1,3 dipolar cycloaddition.[26] The charge density of the cyclobutyl group is consistent with the band structure; molecular levels of the olefin hybridize with nanotube levels away from the Fermi level. The pristine (15,0) SWNT has a nonzero band gap, which increases by 0.1 eV after olefin functionalization.

In the cases of metallic nanotubes, we find that the original $\pi-\pi^*$ band crossing of metallic armchair and semimetallic tube is disrupted by sidewall functionalization. A band gap opens up, converting metallic tubes to semiconducting tubes. This effect can be understood by the breaking of nanotube mirror symmetry due to strong tube-olefin interactions. This peculiar feature is present in the electronic band structure of the PMDE- and PSEPVE-functionalized armchair nanotube (8,8) (top row of Figure 4). The addition of one olefin to a C−C bond slanted to the tube axis introduces a gap at the band center (Γ point) at the Fermi level, thus making the tube semiconducting. However, addition to a segment perpendicular to the tube axis maintains the symmetry.[27] The band degeneracy in the

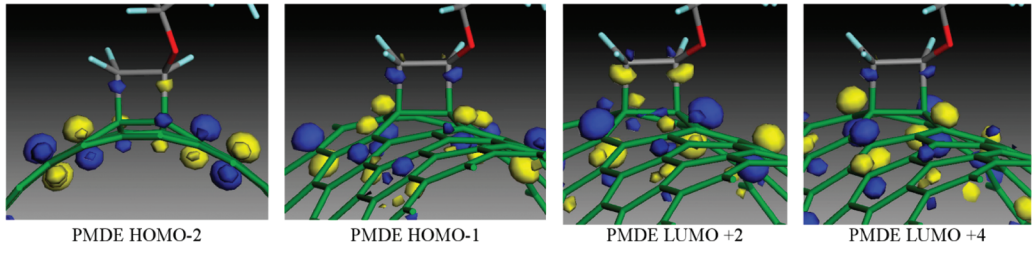

Figure 5. Calculated charge density for PMDE olefin-functionalized (15,0) tube. Left to right: HOMO-2, HOMO-1, LUMO+2, and LUMO+4. In each frame, the charge density is localized at the adduct.

dx.doi.org/10.1021/mz300091v | ACS Macro Lett. 2012, 1, 524−528

pristine SWNT is partially removed by the perturbation from the functional group.

For nanotube (14,0), the valence π-bonding and conduction π^*-antibonding states are along the tube. The LUMO is π^*-antibonding and is also above and below the plane of the tube surface. For tube (15,0), the valence state has two sets of orbitals at the band center: (i) the orbitals that occupy the bond slanted to the tube axis are π-bonding; (ii) those that occupy the C−C bond parallel to the tube axis are π^*-antibonding. The (15,0) conduction state has π-bonding orbitals on the C−C bond parallel to the tube axis. For the (8,8) tube, the orbitals resemble that of the (15,0) tube. The HOMO of the (8,8) tube has two sets of orbitals: the C−C bond slanted to the tube axis is π-bonding, while the C−C bond perpendicular to the tube axis is π^*-antibonding. The LUMO for (8,8) also has two kinds of orbitals: the C−C bond slanted to the tube axis is π^*-antibonding, while the C−C bond perpendicular to the tube axis is π-bonding. The interaction of the olefin HOMO and LUMO with the nanotube surface localizes the symmetry-allowed valence and conduction states of the nanotube; resulting in the simultaneous formation of two new σ bonds. In comparison with [2 + 1] cycloaddition counterpart, the [2 + 2] cycloaddition leads to enhanced level hybridizations, which is important for the gap opening.[12,28−30] The reactive π orbital of olefin plays an important role as the more-constrained benzyne π-system keeps the metallic state intact.[28] Furthermore, the composition dependence of the gap becomes weaker as the extracted band gap for doubling the [2 + 2] adducts yields a moderate (about 10%) increase, in contrast to the [2 + 1] cycloaddtion case where a nearly proportional increase is found.[12]

In summary, we calculated the stability of a [2 + 2] reaction of the PMDE olefin on carbon nanotubes. The random addition of olefins to the metallic (8,8) surface leading to band gap formation is related to the quasi-bound states[31] within the energy gap that originate from the olefin. The formation of these states is particular to divalent additions, in contrast to monovalent functionalizations where localized states are formed.[22] Our results further delineate the essential difference between metallic and semiconducting SWNTs. Band structure analysis is imperative in order to study covalent interactions between molecules and SWNTs because of the associated quantum effect. Our result indicate that scattering centers play little role in the conversion of the metallic features of the mixed mats to semiconducting ones, since π-network disruption features associated with flat bands are not observed in our calculations. The charge density distributions at different k-points reveal that the local symmetry features change with respect to the k-point of the system. The key result is that the symmetry allowed [2 + 2] always exists for metallic nanotubes, albeit not necessarily at the band center. Furthermore, we note that dispersion-corrected approximations are better suited to study these functionalized systems, as evidently demonstrated by the improved binding of dispersion-corrected GGA results over the LDA-VWN ones. These results shed light on the preferential [2 + 2] cycloaddition of olefins to the metallic carbon nanotubes relative to the semimetallic and semiconducting ones.

AUTHOR INFORMATION

Corresponding Author

*E-mail: xwang@cau.edu.

Notes

The authors declare no competing financial interest.

ACKNOWLEDGMENTS

This work was supported by the National Science Foundation (Grant DMR-0934142) and the Air Force Office of Scientific Research (Grant FA9550-10-1-0254).

REFERENCES

(1) Dresselhaus, M. S.; Dresselhaus, G.; Eklund, P. C. *Science of Fullerenes and Carbon Nanotubes: Their Properties and Application*; Academic Press: San Diego, 1996.
(2) Iijima, S. *Nature* **1991**, *354*, 56−58.
(3) Bronikowski, M. J.; Willis, P. A.; Colbert, D. T.; Smith, K. A.; Smalley, R. E. *J. Vac. Sci. Technol., Part A* **2001**, *19*, 1800−1805.
(4) McEuen, P. L. *Phys. World* **2000**, *19*, 31−36.
(5) Tans, S. J.; Devoret, M. H.; Groeneveld, R. J. A.; Dekker, C. *Nature* **1998**, *394*, 761−764.
(6) Ericson, L. M.; Pehrsson, P. E. *J. Phys. Chem. B* **2005**, *109*, 20276−20280.
(7) Ogunro, O. O.; Wang, X.-Q. *Nano Lett.* **2009**, *9*, 1034−1038.
(8) Ju, S. Y.; Doll, J.; Sharma, I.; Papadimitrakopoulos, F. *Nat. Nanotechnol.* **2008**, *3*, 356−362.
(9) An, L.; Fu, Q.; Lu, C.; Liu, J. *J. Am. Chem. Soc.* **2004**, *126*, 10520−10521.
(10) Yi, W.; Malkovskiy, A.; Chu, Q.; Sokolov, A. P.; Colon, M. L.; Meador, M.; Pang, Y. *J. Phys. Chem. B* **2008**, *112*, 12263−12269.
(11) Chen, Y.; Malkovskiy, A.; Wang, X.-Q.; Lebron-Colon, M.; Sokolov, A. P.; Perry, K.; More, K.; Pang, Y. *ACS Macro Lett.* **2012**, *1*, 246−251.
(12) Suggs, K.; Reuven, D.; Wang, X.-Q. *J. Phys. Chem. C* **2011**, *115*, 3313−3317.
(13) Fagan, S. B.; da Silva, A. J. R.; Mota, R.; Baierle, R. J.; Fazzio, A. *Phys. Rev. B* **2003**, *67*, 033405.
(14) Tournus, F.; Charlier, J.-C. *Phys. Rev. B.* **2005**, *71*, 165421.
(15) Delaney, P.; Choi, H. J.; Ihm, J.; Louie, S. G.; Cohen, M. L. *Nature* **1998**, *391*, 466−468.
(16) Bettinger, H. F.; Kudin, K. N.; Scuseria, G. E. *J. Am. Chem. Soc.* **2001**, *123*, 12849−12856.
(17) Kanungo, M.; Lu, H.; Malliaras, G. G.; Blanchet, G. B. *Science* **2009**, *323*, 234−237.
(18) Vosko, S. H.; Wilk, L.; Nusair, M. *Can. J. Phys.* **1980**, *58*, 1200−1211.
(19) Perdew, J. P.; Burke, K.; Ernzerhof, M. *Phys. Rev. Lett.* **1996**, *77*, 3865−3868.
(20) Ouyang, M.; Huang, J. L.; Cheung, C. L.; Lieber, C. M. *Science* **2001**, *292*, 702−705.
(21) Ouyang, M.; Huang, J.-L.; Lieber, C. M. *Annu. Rev. Phys. Chem.* **2002**, *53*, 201−220.
(22) Park, H.; Zhao, J.; Lu, J. P. *Nanotechnology* **2005**, *16*, 635−638.
(23) Vogelsanger, B.; Caminati, W.; Bauder, A. *Chem. Phys. Lett.* **1987**, *141*, 245−250.
(24) Egawa, T.; Fukuyama, T.; Yamamoto, S.; Takakbayashi, F.; Kambara, H.; Ueda, T.; Kuchitsu, K. *J. Chem. Phys.* **1987**, *86*, 6018−6026.
(25) Zhao, J.; Park, H. K.; Han, J.; Lu, J. P. *J. Phys. Chem. B* **2004**, *108*, 4227−4230.
(26) Cho, E.; Shin, S.; Yoon, Y.-G. *J. Phys. Chem. C* **2008**, *112*, 11667−11672.
(27) Britz, D. A.; Khlobystov, A. N. *Chem. Soc. Rev.* **2006**, *35*, 637−659.
(28) Denis, P. A.; Iribarne, F. *J. Mater. Chem.* **2012**, *22*, 5470−5477.
(29) Denis, P. A.; Iribarne, F. *J. Phys. Chem. C* **2011**, *115*, 195−203.
(30) Suggs, K.; Person, V.; Wang, X.-Q. *Nanoscale* **2011**, *3*, 2465−2468.
(31) Veloso, M. V.; Filho, A. G. S.; Filho, J. M.; Fagan, S. B.; Mota, R. *Chem. Phys. Lett.* **2006**, *430*, 71−74.